I&EC research
Industrial & Engineering Chemistry Research

pubs.acs.org/IECR
Article

Glycerol Hydrogenolysis Goes SMART—Separating Reaction Steps as a Key for Tailoring Selectivity and Reaction Control

Published as part of Industrial & Engineering Chemistry Research special issue "Smart Reactors—Towards Adaptive, Resilient, and Autonomous Process Systems".

Piet Hassenstein, Jan-Dominik H. Krueger, Leandros Paschalidis, Dorothea Voß, Mirko Skiborowski, and Jakob Albert*

Cite This: https://doi.org/10.1021/acs.iecr.6c00905

Read Online

ACCESS | Metrics & More | Article Recommendations | Supporting Information

ABSTRACT: The next generation of flexible, efficient, and robust chemical processes requires adaptive, resilient, and autonomous process systems that drive the transition from fossil to renewable feedstocks as one of the central challenges in building climate-neutral and sustainable chemical value chains. One central element will be the next generation of reactors that are SMART—Sustainable, Multipurpose, Autonomous, Resilient, and Transferable—merging process engineering with materials science, analytics, electronics, and data science. Herein, the chemical hydrogenolysis of glycerol to 1,2-propanediol (1,2-PDO) was used as a case study for tailoring selectivity and reaction control by coupling modeling with experimental approaches for process control, demonstrating adaptive reactor behavior. In detail, the reaction was split into a high-temperature step for the endothermic glycerol dehydration under an inert atmosphere and a consecutive low-temperature step under a hydrogen atmosphere, optimizing the reaction conditions for both reactions and deducing individual kinetic parameters by a graphical analysis of one-factor-at-a-time variations and a global nonlinear regression for the temporal concentration data. The results yield a reaction order of around 0.27 for glycerol with an activation energy of 43 kJ mol^{-1} for the dehydration step as well as reaction orders of zero for acetol and around 2.15 for hydrogen at an activation energy of 57 kJ mol^{-1} for the hydrogenation step. The simulated concentration profiles highlight the good agreement between the model and the experimental data. This allows for the implementation of the two-step reaction in a SMART reactor, strengthening the vision of a future generation of autonomous, resilient, and transferable process systems.

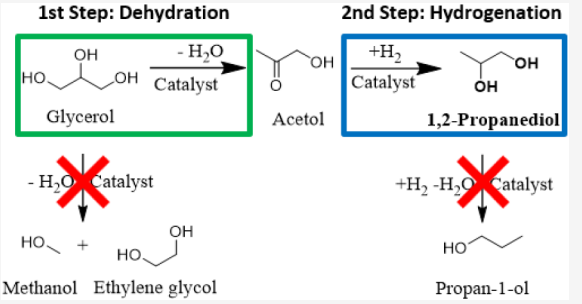

INTRODUCTION

Biofuel production has increased significantly over the past decade, driven by the need to defossilize industry, agriculture, and transportation.[1] Biodiesel, which is produced through the transesterification of triglycerides with methanol, is one of the most important alternative fuels. Naturally, this increased demand results in augmented production of the main side product glycerol, which accounts for around 10 wt % of the biodiesel production output. As production increases, glycerol becomes cheaper, enabling new applications that were previously uneconomical.[2]

Purified glycerol is used in cosmetics, food, and pharmaceuticals. However, crude glycerol from biodiesel production contains significant impurities. These impurities, including water, ash, and soap, can account for up to 40% of the crude glycerol's weight, making it unsuitable for use in most industries without expensive purification.[3] For this reason, the low-cost crude glycerol can serve as a biobased platform for producing value-added chemicals such as acrolein,[4] 1,3-propanediol,[5] and 1,2-propanediol (1,2-PDO).[6−8] 1,2-PDO is a platform chemical with various applications like polyester production, pharmaceuticals, cosmetics, food, and animal feed, or as an antifreeze agent.[8] Producing 1,2-PDO from crude glycerol would be a sustainable and climate-friendly approach, reducing the need for energy-intensive purification steps like in the state-of-the-art petrochemical-based production process.[9]

The complex reaction network for glycerol hydrogenolysis to 1,2-PDO contains several parallel and consecutive reaction steps and was investigated in detail by Gatti et al.[10] and Dasari et al.[11] Moreover, separating the glycerol hydrogenolysis reaction into two steps (Figure 1), initial glycerol dehydration to acetol under a nitrogen atmosphere at high temperature,

Received: February 27, 2026
Revised: May 18, 2026
Accepted: May 19, 2026

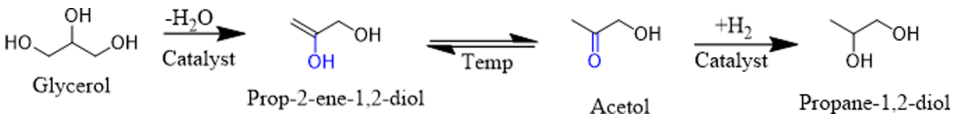

Figure 1. Simplified reaction scheme based on the optimized procedure described by Hassenstein et al.[12]

followed by acetol hydrogenation to 1,2-PDO under a hydrogen atmosphere at low temperature, drastically simplifies the reaction scheme and can lead to higher overall yields and almost perfect selectivity for 1,2-PDO.[12]

The main steps of glycerol hydrogenolysis and the most prominent side reaction are summarized in Scheme 1, along with their corresponding reaction enthalpies. Herein, the dehydration of glycerol to acetol is slightly endothermic,[13] whereby the consecutive hydrogenation of 1,2-PDO is exothermic.[14] However, the undesired initial C−C cleavage reaction of glycerol to ethylene glycol is also exothermic.[15]

Scheme 1. Main Reaction Steps and Major Side Reaction for the Glycerol Hydrogenolysis Reaction[13,14]

$$C_3H_8O_3 \rightleftharpoons C_3H_6O_2 + H_2O \quad \Delta H_R^{\ominus} = 0.32 \text{ kJ mol}^{-1}$$

$$C_3H_6O_2 + H_2 \rightleftharpoons C_3H_8O_2 \quad \Delta H_R^{\ominus} = -64.30 \text{ kJ mol}^{-1}$$

$$C_3H_8O_3 \rightleftharpoons C_2H_6O_2 + CH_3OH \quad \Delta H_R^{\ominus} = -28.80 \text{ kJ mol}^{-1}$$

Typically, Ru- and Cu-containing catalysts impregnated on various carbon supports are discussed as the most efficient for selective glycerol hydrogenolysis to 1,2-PDO as carbon-based supports are superior compared to classical metal oxides, providing the necessary high specific surface area to disperse metal particles effectively, thereby increasing activity.[15−18] Moreover, carbon-based supports tend to exhibit higher stability and do not undergo hydrothermal alterations compared to traditional metal oxide supports.[19] Comparing various carbon supports, Ru-based catalysts tend to be more active if supported on carbon nanotubes (CNTs) rather than on active carbon, due to an increased amount of the electron-rich $Ru^{\delta-}$ species, favoring the terminal C−O cleavage.[20]

Sherbi et al.[21] reported a bimetallic Ru−Cu catalyst supported on CNTs via a classical wetness-impregnation method. Adding Cu promoted the C−O cleavage over undesired C−C cleavage leading to ethylene glycol formation, which is catalyzed by purely Ru-based catalysts. This resulted in a selectivity for 1,2-PDO of up to 93.4%; however, the catalyst showed only a moderate activity. Moreover, Lumpp et al.[22] further improved the performance of the Ru−Cu/CNT catalyst by altering the metal ratio of Ru:Cu with the help of a data-driven model producing a $RuCu_3$/CNT catalyst combining both high activity (X = 78%) and high 1,2-PDO selectivity (S = 79%).

Most kinetic studies for glycerol hydrogenolysis have so far focused on the conventional batch process at high temperatures (>200 °C) and high hydrogen pressures (>30 bar).[23−27] In this approach, glycerol dehydration to acetol and hydrogenation of acetol to 1,2-PDO occur simultaneously. However, as both reaction steps require significantly different reaction conditions with respect to both the gas atmosphere (inert for glycerol dehydration to prevent undesired C−C cleavage and moderate hydrogen atmosphere for the consecutive hydrogenation to 1,2-PDO to prevent further hydrogenolysis and decarboxylation) and reaction temperature (high for endothermic glycerol dehydration versus low for the exothermic glycerol hydrogenolysis), separating both reaction steps would allow for an individual optimization and therefore process intensification.

In a previous study it could be demonstrated that the C−C cleavage and subsequent hydrogenolysis can be prevented by splitting the reaction into two steps.[12] The first step, the dehydration of glycerol to acetol, is conducted at high temperatures (>200 °C) under a pure nitrogen atmosphere. This allows glycerol dehydration to acetol with very high selectivity, efficiently preventing CC cleavage, which only occurs in the presence of hydrogen. The second step is conducted at low temperatures (<150 °C) in the presence of hydrogen. At these reaction conditions, the lower temperature prevents C−C cleavage and subsequent hydrogenolysis. This is an approach similar to the one suggested by Chiu et al.,[28] who achieved acetol selectivities over 90% by conducting the reaction under nitrogen and removing acetol via reactive distillation.

Several studies focused on the competing hydrogenolysis of glycerol to 1,2-PDO and the C−C cleavage to ethylene glycol.[23,26] Pandhare et al.[26] modeled the hydrogenolysis reaction using both a power-law and a Langmuir−Hinshelwood−Hougen−Watson (LHHW) model. The LHHW model yielded the best estimate, with an activation energy of 88.2 kJ mol^{-1} and a reaction order with respect to glycerol of 1.2. Gabrysch et al.[23] used a power-law model and reported a higher activation energy of 106 kJ mol^{-1}, a zero-order dependence on glycerol, and a first-order dependence on hydrogen. Vasiliadou and Lemonidou[25] examined the competing formation of 1,2-PDO and 1,3-PDO over a Cu/SiO_2 catalyst using a power-law model. For 1,2-PDO, they reported reaction orders of 0.27 in glycerol and 0.95 in hydrogen. The 1,3-PDO route showed a glycerol order of 2.4 and a hydrogen order that dropped from about 0.94 at 20−60 bar to nearly zero above 60 bar. What all of these studies have in common is that they focused on the conventional one-step approach.

Consequently, this study aims for the detailed kinetic investigation of the two separate reaction steps, initial glycerol dehydration followed by consecutive acetol hydrogenation, using a highly efficient Ru−Cu/CNT catalyst based on previous studies.[12,22] Moreover, a kinetic model allowing for the precisely determining quantitative reaction parameters will be set up that lays the basis for the future implementation of the two-step reaction in a SMART reactor.

MATERIALS AND METHODS

Materials

All materials were bought and used without purification. As reactants, glycerol from Alfa Aesar (+99%), acetol from Thermo Scientific (+95%), high purity acetol from KremsChem Austria GmbH (+98%), and 1,2-PDO from Sigma-Aldrich (99%) were used. H_2 (5.0 grade, Linde) and N_2 (5.0 grade, Linde) were used for the kinetic experiments. NANOCYL NC7000 carbon nanotubes by Nanocyl SA were used as the catalyst support. $RuCl_3 \cdot 3H_2O$ and $Cu(II)(NO_3)_2 \cdot 3H_2O$, both purchased from Sigma−Aldrich, were used for the catalyst synthesis.

https://doi.org/10.1021/acs.iecr.6c00905
Ind. Eng. Chem. Res. XXXX, XXX, XXX−XXX

Catalyst Synthesis

The synthesis of the Ru−Cu/CNT powder catalyst is already described by the wetness impregnation method introduced by Sherbi et al.[21] The metal precursors were dissolved separately in a total of 820 mL of water and then added to NANOCYL NC7000 carbon nanotubes. The resulting suspension was heated to 80 °C and stirred at 100 rpm using a rotary evaporator for 5 h. Afterward, water was removed under reduced pressure. The obtained powder was gently ground and dried in an oven (Nabertherm L9/11) at 110 °C for 8 h. Prior to use, the catalyst was reduced in a tube furnace (Nabertherm R50/250/12) under forming gas containing 5 vol % hydrogen in nitrogen at 550 °C for 8 h, with a heating rate of 120 K h^{-1} and a gas flow of 50 L h^{-1}. The catalyst was then stored under an argon atmosphere until use.

Reactor Setup for the Kinetic Experiments

Experiments for both reaction steps, glycerol dehydration and acetol hydrogenation, were carried out in a 300 mL stirred-tank reactor (STR, Parr Instrument) fitted with a gas-entrainment stirrer (Figure S1). The reactor, pipes, and valves were made of stainless steel (1.4571), and all sealing elements were made of PTFE. Temperature control was achieved through a type K thermocouple inside a stainless-steel housing, a heating mantle (Parr Instrument), and an external thermostat (Peter Huber Kältemaschinenbau SE). Gas pressures were adjusted manually via ball-and-needle valves, and system pressure was monitored using both analog and digital gauges. Liquid samples collected before, during, and after the reaction were examined by high-performance liquid chromatography (HPLC) using a Nexera 40 system (Shimadzu) to quantify liquid-phase substances. Prior to injection, each sample was filtered through a 0.45 μm syringe filter. Measurements were carried out at 25 °C with a mobile-phase flow of 0.8 mL min^{-1} consisting of an aqueous sulfuric acid solution at 4 mmol L^{-1}. Analysis was performed using a polymer-based organic acid column (300 mm × 8 mm, Chromatographie-Service GmbH). A refractive index detector (RID) was used for detection. Calibration of all identified products had been completed previously, as illustrated in Figure S2. An online gas chromatograph (Bruker 450 GC) was connected to the reactor via heated transfer lines maintained at 200 °C to prevent condensation of reactants and products. The GC setup contained two flame ionization detectors (FID), one thermal conductivity detector (TCD), a methanizer, and four chromatographic columns (Restek Q-Bond, Restek U-Bond, Bruker Swax, Bruker Molsieve 5Å) to enable detailed gas-phase analysis.

Experimental Procedure

In a typical experiment, 1.00 g of catalyst was introduced into the reactor together with 150 mL of the reaction solution. In a typical experiment for the first glycerol dehydration step, a standard solution containing 20 wt % glycerol in water was employed. In contrast, a lower acetol concentration (7.5 wt %) was selected for the hydrogenation step to mimic the desired glycerol conversion from the first step. After the reactor was sealed, the stirring speed was set to 300 rpm. The system was then purged once with 20 bar of nitrogen at ambient temperature to eliminate residual air. Subsequently, two additional purge cycles were performed using either 20 bar of hydrogen or nitrogen, depending on the experimental conditions. The reactor was then pressurized with hydrogen, nitrogen, or a defined mixture of the two gases to the required initial pressure. The total pressure prior to heating was fixed at 30 bar. A minimum nitrogen partial pressure of 5 bar at room temperature was always maintained to prevent the boiling of the reaction mixture in the event of complete hydrogen consumption. Then, the target temperature was set. Upon reaching the desired temperature, the reaction was initiated by increasing the speed of the gas entrainment stirrer to 1000 rpm.

Liquid samples for HPLC analysis and gas samples for online GC were collected via a riser tube connected to a filter throughout the reaction. For the standard dehydration reaction, liquid samples were collected at the start and at 15 min intervals for the first hour, at 30 min intervals for the second hour, and thereafter at hourly intervals until the reaction was stopped after a total duration of 7 h. GC measurements were performed every 30 min for the first 2 h and then once per hour until termination. During acetol hydrogenation, liquid samples were taken every minute during the first 5 min, every 5 min until 15 min had elapsed, and then every 15 min until the experiment was terminated after 1 h. GC samples were taken at the same intervals as liquid samples whenever feasible. Due to the extended GC analysis time (23 min), gas-phase characterization was limited to one measurement every 30 min.

Determination of the Kinetics and Calculations

For the analysis and modeling of the reaction kinetics, two approaches were applied, building on a graphical analysis of one-factor-at-a-time variations (OFAT) and a nonlinear regression (NLR) that simultaneously accounts for all experiments. For the OFAT approach, the effect of individual variations in temperature or substrate concentrations was derived by analyzing the reaction rate by plotting the reactant concentrations over time and applying a linear fit. To determine the reaction order, we plotted the natural logarithm of the reaction rate against the initial reactant concentrations. A linear fit was then applied, and the slope of this line provided the reaction order. OriginPro 2025 (OriginLab) was used to plot the data and perform the regression analyses. The results are described in the following section in alignment with Figures 3, 5, 8, and 10.

In order to model the hydrogen solubility, the COSMO*therm* software was used with the parametrization TZVPD_FINE for the COSMO-RS estimation. Quantum-chemical input data were generated using Turbomole[29] in combination with COSMO*conf*.[30] The methodology used is shown in the Supporting Information (Section: Methodology for the Estimation of Hydrogen Solubility in Water-Acetol and Water-Glycerol Mixtures Using COSMO-RS).

The following calculations were used to determine the reactant conversion (eq 1), product yield (eq 2), 1,2-PDO selectivity (eq 3), overall carbon balance (eq 4), turnover frequency (TOF, eq 5), turnover number (TON, eq 6) and atomic efficiency (eq 7):

$$X = \frac{c_{0,i} - c_i}{c_{0,i}} \times 100 \tag{1}$$

$$Y_i = \frac{c_i}{c_{0,i}} \times 100 \tag{2}$$

$$S_i = \frac{Y_i}{X} \times 100 \tag{3}$$

$$C_{\text{balance}} = \frac{\sum n_i \times \text{number of carbons}}{n_{0,\text{reactant}} \times 3} \times 100 \tag{4}$$

$$\text{TOF} = \frac{m_{\text{Product}}}{m_{\text{active metal}} \times t} \tag{5}$$

$$\text{TON} = \frac{n_{\text{Product}}}{n_{\text{active metal}}} \tag{6}$$

$$\text{atomic efficiency} = \frac{n_{\text{desired product}}}{n_{\text{reacted reactant}}} \times 100 \tag{7}$$

The Arrhenius plot was used to determine the activation energy from the temperature variation experiments. The Arrhenius plot is derived from the Arrhenius equation (eq 8) by applying a natural logarithm (eq 9)

$$k = A \cdot e^{-\frac{E_a}{RT}} \tag{8}$$

$$\ln(k) = \ln(A) - \frac{E_a}{R} \cdot \frac{1}{T} \tag{9}$$

Henry's law was used to determine the concentration of the dissolved hydrogen in the reaction liquid and is shown in eq 10

$$c_{H_2,\text{dis}} = H_s^{\text{cp}} \cdot p_{H,2} \tag{10}$$

https://doi.org/10.1021/acs.iecr.6c00905
Ind. Eng. Chem. Res. XXXX, XXX, XXX−XXX

To investigate whether the reaction is externally heat-transfer-limited, the Mears criterion[31] for external heat-transfer limitations, shown in eq 11, was applied

$$\frac{|\Delta H_R| \cdot r \cdot R \cdot E_A}{h \cdot T_b^2 \cdot R_g} < 0.15 \tag{11}$$

With ΔH_R as the reaction enthalpy, r as the reaction rate, R as the catalyst radius, E_A as the activation Energy, h as the heat transfer coefficient, T_b as the bulk temperature, and R_g as the universal gas constant.

The dehydration reaction was modeled as irreversible, following mass-action kinetics, with the rate constant described by the Arrhenius equation. The reaction rate is given by eq 12

$$r_{GD} = k_{0,GD} \cdot e^{\left(-\frac{E_{A,GD}}{R \cdot T}\right)} \cdot C_G^{n_{GD}} \tag{12}$$

where r_{GD} is the reaction rate, $k_{0,GD}$ is the pre-exponential constant, $E_{A,GD}$ is the activation energy, T is the temperature, C_G is the concentration of glycerol, and n_{GD} is the reaction order with respect to glycerol.

The hydrogenation reaction was modeled as irreversible, following mass-action kinetics, with the rate constant described by the Arrhenius equation. The reaction rate is given by eq 13

$$r_{HPH} = k_{0,HPH} \cdot e^{\left(-\frac{E_{A,HPH}}{R \cdot T}\right)} \cdot C_H^{n_{HPH}} \tag{13}$$

where r_{HPH} is the reaction rate, $k_{0,HPH}$ is the pre-exponential constant, $E_{A,HPH}$ is the activation energy, T is the temperature, C_H is the concentration of dissolved hydrogen, and n_{HPH} is the reaction order with respect to glycerol.

For the NLR, a detailed description for both the kinetic models and the specific parameter estimation can be found in the Supporting Information in the Sections: Methodology for the Kinetic Model for the Dehydration of Glycerol and Methodology for the Kinetic Model for the Hydrogenation of Acetol.

RESULTS AND DISCUSSION

Based on previous studies deducing the detailed kinetics and emphasizing a kinetic model for the one-step chemical hydrogenolysis of glycerol to 1,2-PDO using a multifunctional Ru−Cu/CNT catalyst,[12,22] the two reaction steps require drastically different reaction conditions with respect to both gas atmosphere and temperature range.[12] The key feature for making the glycerol hydrogenolysis reaction "SMART" is to separate both reaction steps in one single unit operation using the same catalyst that allows for tailoring both selectivity and reaction control. For identifying suitable tools to make glycerol hydrogenolysis adaptable, the kinetics of the individual subreactions have to be determined first to allow for rigorous suggestions for process intensification. For the purpose of kinetic modeling, experiments were conducted at different initial hydrogen pressures, substrate concentrations, and temperatures, wherein all the liquid- and gas-phase products were analyzed as a function of time. Since the presence of gas-phase products is not convenient for sampling in batch reactors, a batch-slurry reactor was used in this study (Figure S1), wherein the experiments with the same initial conditions were conducted for different time durations.

1st Step: Kinetics of the Dehydration of Glycerol to Acetol

In a previous study, external mass-transfer limitations could be excluded during a stirrer speed variation between 400 and 1200 rpm showing no significant changes of the initial reaction rate;[12] being in good agreement with analogous studies carried out by Torres et al.[24] and Sharma et al.[27] Moreover, varying the catalyst mass using the same Ru−Cu/CNT catalyst between 200 mg and 1000 mg, resulted in a linear relation with the reaction rate proving the absence of external mass-transfer limitations.[12] As far as internal particle diffusion is concerned, catalyst particles in powder form (typically less than 50 μm), as those used in the present study, ensure insignificant internal diffusion resistance.[22,26]

To determine the reaction order of glycerol during the first dehydration step (Figure 1), the initial glycerol concentration was varied from 5 to 40 wt % in an aqueous solution applying an inert nitrogen atmosphere to suppress the undesired C−C cleavage leading to ethylene glycol formation deduced from a previous study.[12] Reproducibility experiments (Table S1) confirmed the standard deviation to ±1.9% for glycerol conversion, to ±0.2% for acetol yield, and to ±1.7% for acetol selectivity, as well as to ±0.9% for the overall carbon balance. Figure 2 shows that the initial glycerol concentration has only a

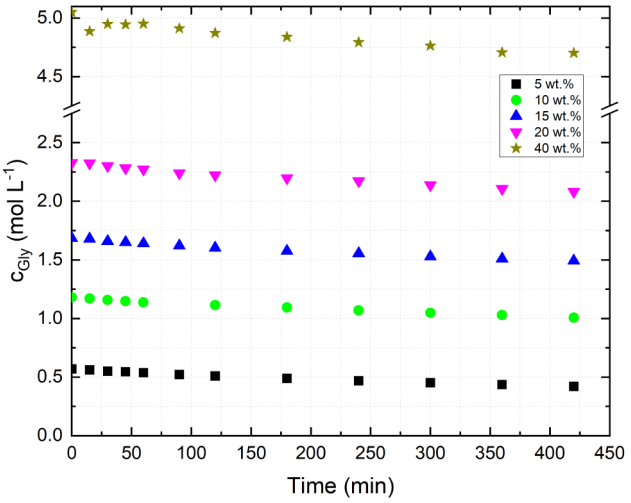

Figure 2. Temporal profiles for glycerol concentration at varying initial amounts of glycerol. Reaction conditions: V = 150 mL, T = 220 °C, $p_0(N_2)$ = 30 bar, t = 7 h, $N_{stirrer}$ = 1000 rpm, $m_{catalyst}$ = 1.00 g, solvent: H_2O.

negligible effect on the dehydration kinetics. This is supported by the temporal concentration profiles in Figure S3, illustrating the linear fit used to determine the reaction rate. The data indicate that the reaction rate increases only marginally from 0.35 mmol L^{-1} min^{-1} at 5 wt % glycerol to 0.70 mmol L^{-1} min^{-1} at 40 wt % glycerol.

Figure 3 plots the natural logarithm of the determined reaction rates versus the corresponding natural logarithm of the initial glycerol concentrations. As the initial glycerol concentration increases, the reaction rate increases. A reaction order with respect to glycerol n_{GD} of 0.27 ± 0.05 was determined. This is the same reaction order reported by Vasiliadou and Lemonidou[25] for glycerol hydrogenolysis using a Cu/SiO_2 catalyst.

Figure 4 shows the glycerol conversion (X), acetol yield (Y), and acetol selectivity (S) for the glycerol dehydration step, resulting from the corresponding temporal profiles shown in Figure S4. As expected for a chemical reaction with a reaction order below 1, the glycerol conversion decreases from 26% at 5 wt % to 6.9% at 40 wt % glycerol. The acetol yield also decreases with increasing glycerol concentration, from 11% at 5 wt % to 3.3% at 40 wt % glycerol. However, a different trend was observed for acetol selectivity. First, the latter increases

https://doi.org/10.1021/acs.iecr.6c00905
Ind. Eng. Chem. Res. XXXX, XXX, XXX−XXX

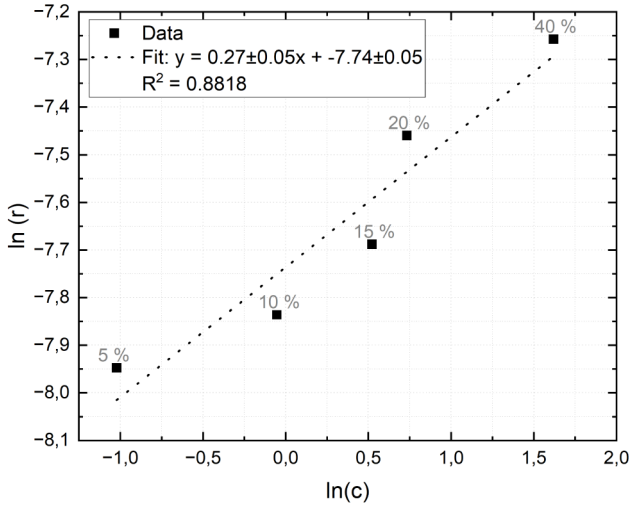

Figure 3. Graphical determination of the reaction order for different initial glycerol concentrations in the dehydration step. Reaction conditions: V = 150 mL, T = 220 °C, $p_0(N_2)$ = 30 bar, t = 7 h, $N_{stirrer}$ = 1000 rpm, $m_{catalyst}$ = 1.00 g, solvent: H_2O.

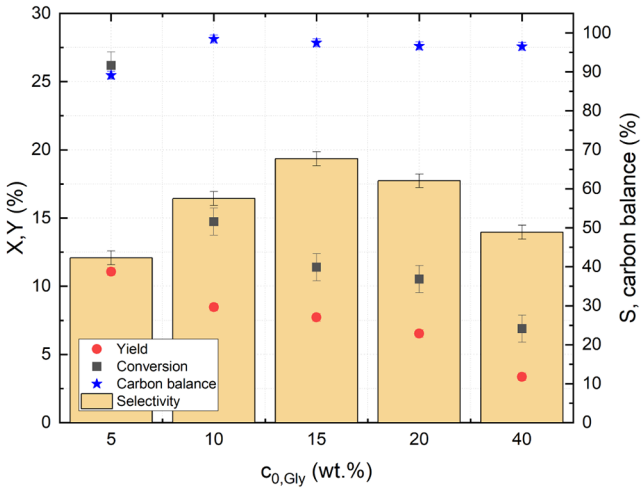

Figure 4. Overview of glycerol conversion (X), yield (Y), and selectivity (S) of acetol and carbon balance at the end of the kinetic experiments for different initial glycerol concentrations. Reaction conditions: V = 150 mL, T = 220 °C, $p_0(N_2)$ = 30 bar, t = 7 h, $N_{stirrer}$ = 1000 rpm, $m_{catalyst}$ = 1.00 g, solvent: H_2O.

from 42% at 5 wt % glycerol to a maximum of 68% at 15 wt % only to decrease again to 49% at 40 wt % glycerol. High carbon balances of >96% were achieved for all experiments, except for 89% at 5 wt %, most likely due to the overall low amounts, which are close to the detection limit of the used analytics. 15 wt % glycerol was selected as the optimal glycerol concentration for the dehydration step, since it achieves the highest acetol selectivity, while achieving a good compromise between acetol yield and glycerol conversion, allowing for precise reaction control.

The influence of temperature on the glycerol dehydration step was determined by varying the reaction temperature from 220 to 250 °C. The corresponding temporal profiles of the glycerol concentration are shown in Figure S5. As expected for an endothermic reaction (Scheme 1), the reaction rate increases from 0.6 mmol L^{-1} min^{-1} at 220 °C to 1.0 mmol L^{-1} min^{-1} at 250 °C with increasing temperature.

The activation energy was deduced using an Arrhenius plot (Figure 5), whereby the slope of the linear fit yields an

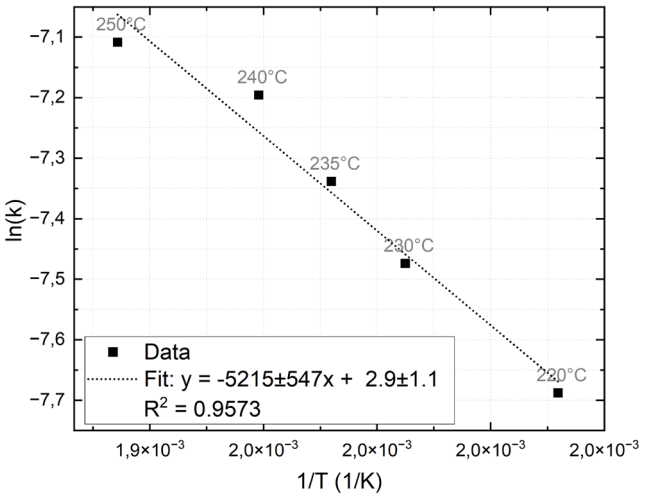

Figure 5. Arrhenius plot to determine the activation energy for the glycerol dehydration step. Reaction conditions: V = 150 mL, $p_0(N_2)$ = 30 bar, t = 7 h, $N_{stirrer}$ = 1000 rpm, $c_{0,Glycerol}$ = 20 wt %, $m_{catalyst}$ = 1.00 g, solvent: H_2O.

activation energy of 43.36 ± 4.5 kJ mol^{-1}, and a pre-exponential factor of $k_{0,GD}$ of 18.17^{+36}_{-12} $M^{0.73}$·min^{-1}. This is significantly lower compared to the single-step glycerol hydrogenolysis reaction reported by Hassenstein et al. using the same Ru−Cu/CNT catalyst with 126.3 kJ mol^{-1},[12] as well as the 84.6 kJ mol^{-1} for a Cu−Pd/TiO_2−Na catalyst reported by Ardila et al.[32] and 96.8 kJ mol^{-1} using a Cu/SiO_2 catalyst reported by Vasiliadou and Lemonidou[25] To determine whether the reaction was externally heat-transfer-limited, the Mears criterion was applied,[31] using the reaction enthalpy for the glycerol dehydration to acetol of 0.316 kJ mol^{-1}, as determined by Zhang et al.[13] A catalyst particle radius of 5.7 × 10^{-10} m according to Lumpp et al.[22] was used. For the heat transfer coefficient, a value of 2000 W K^{-1} was assumed, which represents the lowest thermal conductivity, so the worst-case scenario, given by Han and Fina.[33] According to Mears, if the left side of eq 11 is smaller compared to 0.15, then the temperature of the catalyst surface and the bulk fluid will be the same. The results of the Mears criterion for the temperature variation experiments are summarized in Table S2 confirming that reactions are not externally heat-transfer-limited, since the resulting values are much smaller than 0.15.

Figure 6 shows that an increase in reaction temperature affects not only the reaction kinetics but also the selectivity, as undesired side reactions like glycerol and acetol reforming become more prominent with increasing temperature. The corresponding temporal profiles for conversion (X), acetol yield (Y), and selectivity (S) are shown in Figure S6. While glycerol conversion increases linearly from 10.5% at 220 °C up to 18.4% at 250 °C, a different trend was observed for both acetol yield and selectivity. The acetol yield increases from 6.5% at 220 °C to a maximum of 7.5% at 230 °C to then decreases to a minimum of 3.2% at 250 °C. The selectivity remains constant at 62% at 220 and 230 °C, then decreases to a minimum of 17.6% at 250 °C. Consequently, 230 °C was selected as the optimal reaction temperature, as it results in a

https://doi.org/10.1021/acs.iecr.6c00905
Ind. Eng. Chem. Res. XXXX, XXX, XXX−XXX

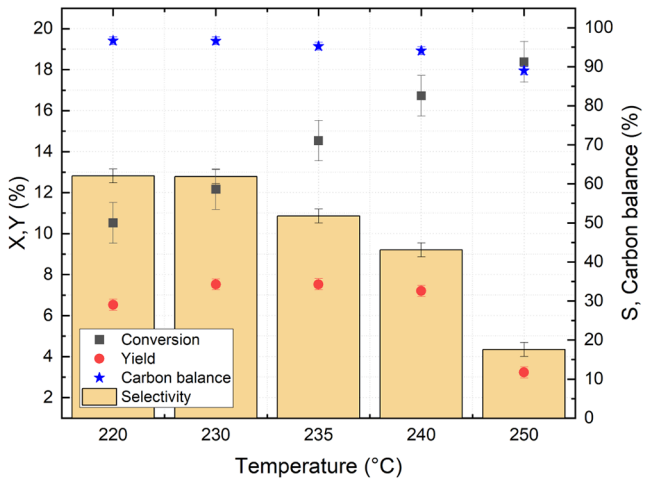

Figure 6. Overview of glycerol conversion (X), yield (Y), and selectivity (S) of acetol and carbon balance at the end of the kinetic experiments for different reaction temperatures. Reaction conditions: V = 150 mL, $p_0(N_2)$ = 30 bar, t = 7 h, $N_{stirrer}$ = 1000 rpm, $c_{0,Glycerol}$ = 20 wt %, $m_{catalyst}$ = 1.00 g, solvent: H_2O.

moderate glycerol conversion with high acetol yield and selectivity.

One reason for the lower acetol selectivity at higher temperatures above 230 °C is the formation of ethanol (Figure S7). While no ethanol was found at reaction temperatures of 220 and 230 °C, ethanol formation resulting from acetol decomposition could be found for higher temperatures. At 235 °C, ethanol is formed after 300 min, with a final yield of 0.86%. At 240 °C, already after 120 min, a significantly higher formation of 2.3% was observed. At 250 °C, ethanol formation was already detected from the beginning throughout the whole experiment, with a maximum yield of 3.6% after 420 min. Ethanol formation from acetol was previously observed by Vikla et al.[34] during aqueous-phase reforming using a supported Pt catalyst at 225 °C and 35 bar.

Another reason for the low acetol selectivity at high temperatures and the lower carbon balance is the poor thermal stability of acetol, forming a highly viscous oil during thermal stability experiments shown in Figure S8.

2nd Step: Kinetics of the Hydrogenation of Acetol to 1,2-PDO

While the dehydration of glycerol is necessary for the formation of 1,2-PDO, it does not directly result in the desired product but only the intermediate acetol (Figure 1). In the second step of the reaction cascade, the hydrogenation of acetol to 1,2-PDO is investigated with respect to reaction orders for both reactants (acetol and H_2), activation energy, as well as optimized parameters for later implementation in a SMART reactor.

To determine the reaction order for hydrogen in the acetol hydrogenation reaction, the hydrogen partial pressure was varied from 5 to 25 bar, while the total pressure was kept constant at 30 bar (the difference was adjusted by inert N_2). Based on the investigations of a previous study,[12] a reaction temperature of 140 °C was selected, avoiding undesired 1,2-PDO decomposition. Herein, solute hydrogen gas diffuses through the gas phase to the gas−liquid interphase and then from the interphase to the bulk liquid. Dissolved hydrogen and acetol present in the liquid phase are then transferred to the external catalyst surface through the solid−liquid film. In order to calculate the concentrations of dissolved hydrogen in the reaction mixtures, COSMO-RS predictions were used to estimate Henry's constant both for water-acetol (Figure S18) as well as water-glycerol mixtures (Figure S19). The resulting temporal profiles for the acetol concentration are shown in Figure 7, and the linear fits are exposed in Figure S9.

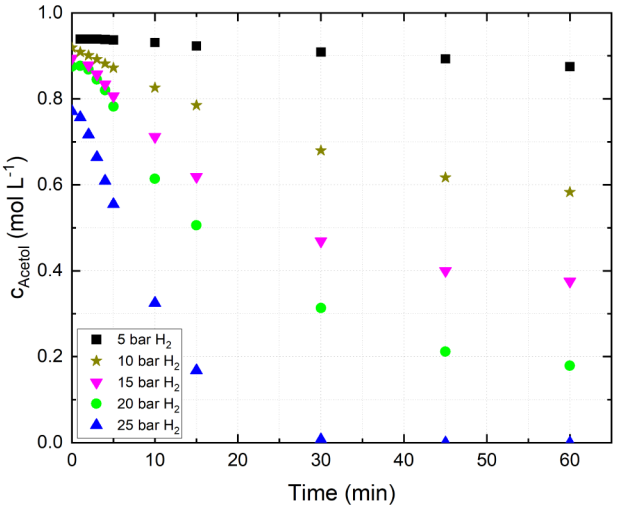

Figure 7. Temporal profiles of the acetol concentration at varying initial hydrogen pressures. Reaction conditions: V = 150 mL, T = 140 °C, p_0(total) = 30 bar, t = 1 h, $N_{stirrer}$ = 1000 rpm, $c_{0,Acetol}$ = 7.5 wt %, $m_{catalyst}$ = 1.00 g, solvent: H_2O.

The acetol concentration decreases more rapidly with higher initial hydrogen partial pressures and in different ways. At 5 bar hydrogen, acetol consumption remains slow and linear, whereas at higher initial hydrogen pressures the reaction accelerates and then slows down due to hydrogen depletion. At 10, 15, and 20 bar, significantly steeper concentration gradients are observed relating to a nonlinear dependency on hydrogen pressure. At 25 bar hydrogen, the steepest gradient for all variations is deduced until all acetol is consumed. The observed differences are due to hydrogen limitations at low pressures. At 5 bar, very little hydrogen is available so that the reaction is limited by the hydrogen availability throughout the reaction. While at 10−25 bar, the reaction is only limited at higher conversion, after most hydrogen has been consumed. This is visible from the flattening of the concentration curve of these reactions. At 25 bar, enough hydrogen is available to fully hydrogenate all of the acetol provided in the kinetic regime, so no limitation is visible. The reaction rate was determined using linear regression. However, only the linear part of the plot was included to avoid the effect of hydrogen limitation, as shown in Figure S9.

Figure 8 plots the natural logarithm of the initial dissolved hydrogen concentrations, which were determined using Henry's law (eq 10), against the natural logarithm of the corresponding reaction rates. As the initial hydrogen concentration increases, the reaction rate also rises. The calculated reaction order n_{HPH} with respect to hydrogen was 2.15 ± 0.20.

Table 1 presents an overview of the kinetic values at the end of the kinetic experiments, together with the calculated TOFs (eq 5) with the corresponding temporal graphs shown in Figure S10. Almost quantitative 1,2-PDO selectivities of >99% were achieved for all initial hydrogen pressures. Acetol

https://doi.org/10.1021/acs.iecr.6c00905
Ind. Eng. Chem. Res. XXXX, XXX, XXX−XXX

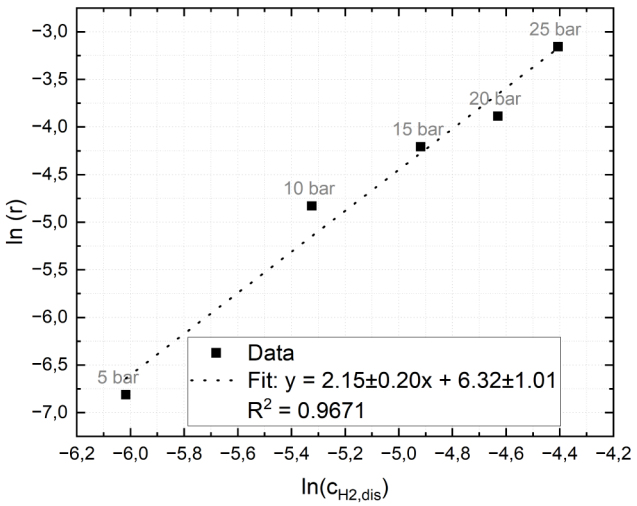

Figure 8. Experimental determination of the reaction order of hydrogen for different initial hydrogen pressures in the 2nd hydrogenation step. Reaction conditions: V = 150 mL, T = 140 °C, p_0(total) = 30 bar, t = 1 h, $N_{stirrer}$ = 1000 rpm, $c_{0,Acetol}$ = 7.5 wt %, $m_{catalyst}$ = 1.00 g, solvent: H_2O.

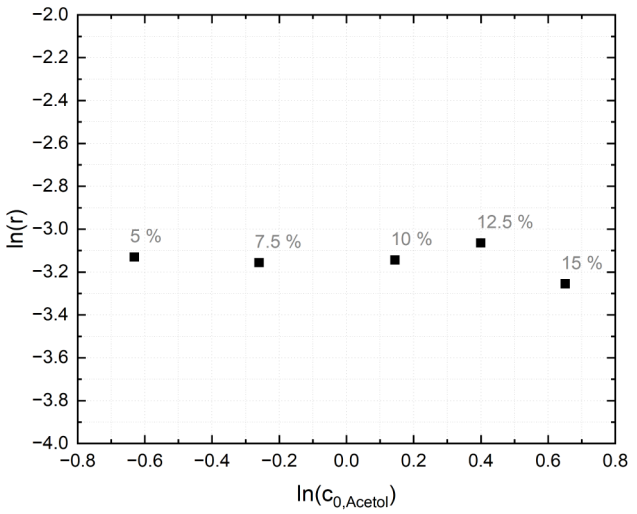

Figure 9. Experimental determination of the reaction order of acetol for different initial acetol concentrations at the 2nd hydrogenation step. Reaction conditions: V = 150 mL, T = 140 °C, $p_0(H_2)$ = 25 bar, $p(N_2)$ = 5 bar, p_0(total) = 30 bar, t = 1 h, $N_{stirrer}$ = 1000 rpm, $m_{catalyst}$ = 1.00 g, solvent: H_2O.

Table 1. Overview of Acetol Conversion, Yield, and Selectivity of 1,2-PDO and TOF and TON at the End of the Kinetic Experiments at Different Initial Hydrogen Pressures[a]

H_2 pressure (bar)	Conversion (%)	Yield (%)	Selectivity (%)	TOF (s^{-1})	TON
5	6.8 ± 1	8.1 ± 0.3	100* ± 2	0.005	18.5
10	36.6 ± 1	38.4 ± 0.3	100* ± 2	0.023	85.8
15	58.1 ± 1	59.1 ± 0.3	100* ± 2	0.037	133.6
20	79.5 ± 1	78.7 ± 0.3	99 ± 2	0.048	175.8
25	100 ± 1	99.4 ± 0.3	99 ± 2	0.059	212.3

[a]The "*" symbol denotes impossible calculated selectivities, due to measurement inaccuracies at low conversions, which were set to 100%. Reaction conditions: V = 150 mL, T = 140 °C, p_0(total) = 30 bar, T = 1 h, $N_{stirrer}$ = 1000 rpm, $c_{0,Acetol}$ = 7.5 wt %, $m_{catalyst}$ = 1.00 g, solvent: H_2O.

conversion and yield strongly depend on the partial pressure of hydrogen. Only at 25 bar hydrogen pressure was complete acetol conversion to 1,2-PDO achieved whereby lower hydrogen pressures limit complete acetol hydrogenation. The results show that 25 bar is the optimal hydrogen pressure, as it not only results in the highest reaction rate, but also achieves complete hydrogenation of acetol to 1,2-PDO. The calculated TOFs after 1 h rise from 0.005 s^{-1} at 5 bar to 0.059 s^{-1} at 25 bar hydrogen, while the TONs increase from 18.5 to 212.3. These increases also show that low hydrogen pressures limit the 519 reaction rate.

To determine the reaction order of acetol in the acetol hydrogenation step, the initial acetol concentration in aqueous solution was varied from 5 to 15 wt % in 2.5 wt % steps, mimicking glycerol conversions achieved in the first dehydration step (see above). The resulting temporal profiles of the acetol concentration and the linear regression used to determine the reaction rate are shown in Figure S11. Similar to the concentration plots for the hydrogen pressure variation, the acetol concentration also flattens out at higher initial acetol concentrations above 10 wt %, indicating a lack of hydrogen for complete hydrogenation. Figure 9 plots the natural logarithm of the initial dissolved hydrogen concentrations against the natural logarithm of the corresponding reaction rates. As the graph shows, acetol hydrogenation is of zero order with regard to acetol.

The final acetol conversion, yield, and selectivity of 1,2-PDO are summarized in the Supporting Information (Table S3), with the corresponding temporal graphs shown in Figure S12. The data also follow the same trend as for the hydrogen pressure variation, with high 1,2-PDO selectivity across all experiments (95.7−100%) and lower acetol conversion and 1,2-PDO yield at higher initial acetol concentrations.

Concerning heat transfer limitations, temperature gradients in the case of liquid-phase systems are typically not so prevalent compared to the vapor phase, as the heat capacities and thermal conductivities of the liquid phase are an order of magnitude higher compared to the gas phase.[23,28] As external heat-transfer limitations could already been excluded for the first glycerol dehydration step using dilute glycerol solutions by the Mears criterion,[31] also dilute acetol solutions were used to reduce heat release for the second hydrogenation step. Therefore, a chemically controlled regime could be assumed and hence true kinetics could be obtained from the experimental data. The influence of temperature on acetol hydrogenation was determined by varying the reaction temperature from 100 to 140 °C in 10 increments. The corresponding temporal acetol concentration plots are shown alongside the linear regressions (Figure S12). All graphs show a rapid decrease in acetol concentration over time. However, the rate of acetol consumption increases with increasing temperature according to Arrhenius' law. At reaction temperatures up to 120 °C, the reaction is not complete after 60 min. Only at 130 and 140 °C all acetol is converted during the reaction time after 60 and 30 min, respectively.

Temperature variation enables graphical determination of the activation energy via an Arrhenius plot, as shown in Figure 10, yielding a calculated activation energy of 57.1 ± 8.9 kJ mol^{-1} and a pre-exponential factor $k_{0,HPH}$ of $7.22^{+103}_{-6.8} \times 10^9$ $M^{-1.15}$ min^{-1}. The determined activation energy is slightly

https://doi.org/10.1021/acs.iecr.6c00905
Ind. Eng. Chem. Res. XXXX, XXX, XXX−XXX

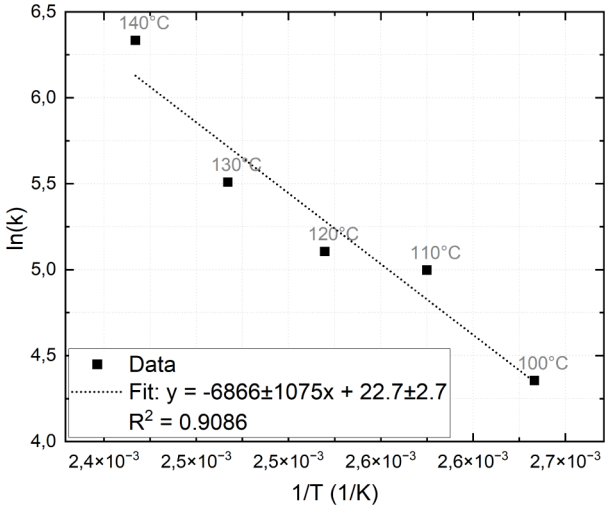

Figure 10. Arrhenius plot to determine the activation energy for the acetol hydrogenation step. Reaction conditions: V = 150 mL, $p_0(H_2)$ = 25 bar, $p(N_2)$ = 5 bar, p_0(total) = 30 bar, t = 7 h, $N_{stirrer}$ = 1000 rpm, $c_{0,Acetol}$ = 7.5 wt %, $m_{catalyst}$ = 1 g, solvent: H_2O.

higher than the 51.2 kJ mol^{-1} reported by Ardila et al.[32] for a Cu−Pd/TiO_2−Na catalyst for glycerol hydrogenolysis.

Although the reaction rate increases with reaction time, 1,2-PDO selectivity remains constantly high, ranging from 95.1% to 99.4%, as shown in the Supporting Information (Table S4), summarizing acetol conversion, 1,2-PDO yield, and 1,2-PDO selectivity of the kinetic experiments, with the corresponding temporal graphs shown in Figure S13.

The difference in selectivity is within the scope of the measurement error. At lower reaction temperatures, lower conversions and yields were achieved, ranging from 48.8% and 46.4% at 100 °C to 88.5% and 86.9% at 120 °C. The final results indicate that both 130 and 140 °C yield quantitative conversion to 1,2-PDO. However, as shown in Figure S12, complete acetol conversion was achieved after 30 min at 140 °C, whereas the same conversion was attained in 60 min at 130 °C.

Kinetic Modeling of the Two-Step Separated Glycerol Hydrogenolysis Reaction

Using experimental data obtained from variations in temperature, reactant concentrations, and hydrogen pressure, kinetic models were developed for both the glycerol dehydration to acetol and the subsequent acetol hydrogenation to 1,2-PDO. The methodology used for the global NLR of the kinetic parameters and the evaluation of confidence intervals and ellipsoids is further outlined in the Supporting Information (Sections: Methodology for the Kinetic Model for the Dehydration of Glycerol; Methodology for the Kinetic Model for the Hydrogenation of Acetol). While an extensive body of literature on the temperature-dependent solubility of hydrogen in pure water is available,[35] reliable data on hydrogen solubility in the water-acetol and water-glycerol mixtures relevant to this work are lacking. Therefore, the quantum-chemistry-based COSMO-RS activity-coefficient model[36−38] was employed to estimate hydrogen solubility in these mixtures to use the resulting information in the kinetic model. Hernández-Bravo et al.[39] have previously shown that the predicted hydrogen solubility in hydrocarbons from COSMO-RS agrees with experimentally determined values. The methodology used to estimate the hydrogen solubility in the acetol-water mixture and the results are also presented in more detail in the corresponding section of the Supporting Information.

The kinetic parameters estimated via NLR for the complete set of time-dependent concentration data for different temperatures and substrate concentrations, as well as those derived by the OFAT analysis based on Figures 3, 5, 8 and 10, are summarized in Table 2. Although the OFAT analysis builds only on a subset of the kinetic data and linear estimation, the parameter estimates of both approaches align exceptionally well for both reactions. Especially the determined activation energies of 42.2 kJ mol^{-1} (NLR) and 43.4 kJ mol^{-1} (OFAT) for the glycerol dehydration and 54.6 kJ mol^{-1} (NLR) and 57.1 kJ mol^{-1} (OFAT) are almost equivalent. The confidence intervals derived from the NLR estimates and especially the confidence ellipsoids (cf. Figures S15 and S16 in the Supporting Information) do however indicate a considerable correlation between the parameters. This is well known and most significant for the pre-exponential factor and the activation energies, which should therefore be interpreted best in combination.

Table 2. Kinetic Parameters Estimated for the Kinetic Model with Nonlinear Regression (NLR) and One-Factor-at-a-Time (OFAT) Analysis for the Glycerol Dehydration to Acetol and the Hydrogenation of Acetol to 1,2-PDO[a]

Kinetic parameter	NLR	NLR—95% confidence interval	OFAT	OFAT—95% confidence interval
$k_{0,GD}$ ($M^{(1-n)}$ min^{-1})	16.48	[2.41, 113.01]	18.17	[6.23, 53.62]
$E_{A,GD}$ (kJ mol^{-1})	42.17	[35.00, 51.00]	43.36	[38.86, 47.86]
n_{GD}	0.16	[0.10, 0.21]	0.27	[0.22, 0.32]
$k_{0,HPH}$ ($M^{(1-n)}$ min^{-1})	8.36 × 10^8	[1.30 × 10^8, 5.37 × 10^9]	7.22 × 10^9	[6.80 × 10^9, 1.03 × 10^{11}]
$E_{A,HPH}$ (kJ mol^{-1})	54.57	[49.53, 60.01]	57.08	[48.2, 66.00]
n_{HPH}	1.82	[1.67, 1.96]	2.15	[1.95, 2.35]
n_{Acetol}	0*	-	0	-

[a]The reaction order regarding acetol for the kinetic model was assumed to be zero, after one-factor-at-a-time analysis.

The remaining difference between the parameter estimates results from the slightly higher reaction orders determined from the OFAT analysis, for which the reaction order is determined graphically from the slope of the linear fit of the logarithm of the reaction rate over the logarithm of the initial substrate composition, from Figures 3 and 8. This analysis builds on the linear fit of the initial temporal concentration profiles, further illustrated in the Supporting Information, while the NLR approach performs a numerical integration of the differential concentration profiles according to the reaction rates, capturing the nonlinearity of the resulting composition profiles. This results in a slightly lower reaction order of 0.16 (NLR) compared to 0.27 (OFAT) for the glycerol dehydration and 1.82 (NLR) compared to 2.15 (OFAT) for the hydrogenation of acetol. This also results in slightly different pre-exponential factors of 16.48 $M^{(1-n)}$ min^{-1} (NLR) compared to 18.17 $M^{(1-n)}$ min^{-1} (OFAT) for the glycerol dehydration and much higher values of 8.36 × 10^8 $M^{(1-n)}$ min^{-1} (NLR) compared to 7.22 × 10^9 $M^{(1-n)}$ min^{-1} (OFAT) for the much faster hydrogenation of acetol. Overall, these

https://doi.org/10.1021/acs.iecr.6c00905
Ind. Eng. Chem. Res. XXXX, XXX, XXX−XXX

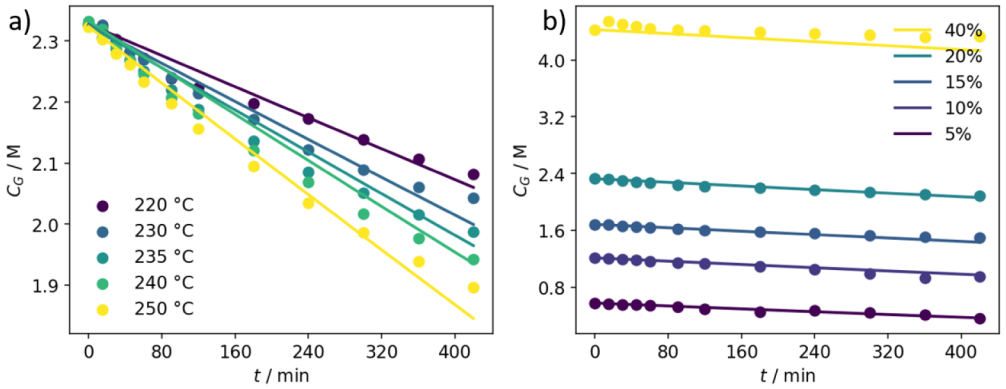

Figure 11. Comparison of the kinetic model with experimental data of the glycerol dehydration for a) temperature variation and b) glycerol concentration variation experiments.

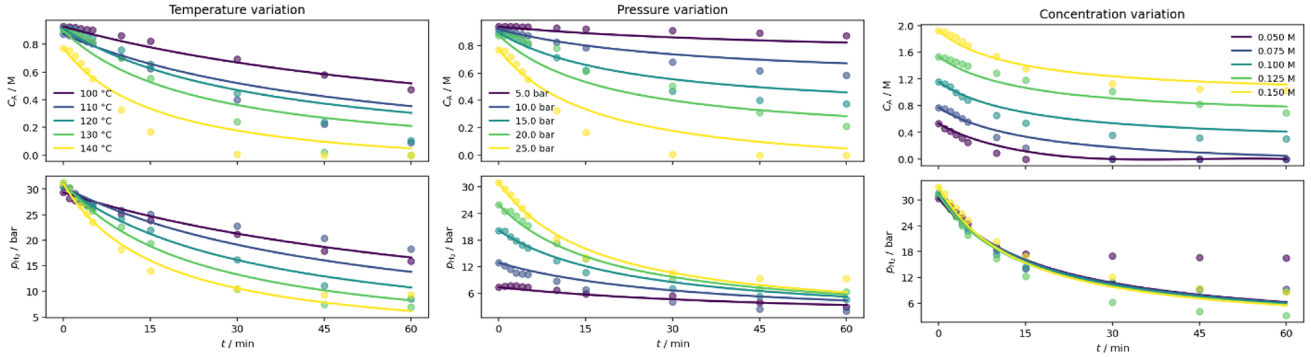

Figure 12. Comparison of the kinetic model of the acetol hydrogenation with the experimental data for temperature variation, hydrogen pressure variation, and the acetol variation experiments.

Table 3. Overview of the Results for the Combined Two-Step Glycerol Hydrogenolysis[a]

Reaction time (min)	Type of atmosphere	Glycerol/Acetol conversion (%)	Acetol yield (%)	1,2-PDO yield (%)	Acetol selectivity (%)	1,2-PDO selectivity (%)	Atomic efficiency (%)
420	N_2	13.4	9.0	0.6	67.0	4.4	71.4
480	H_2	100	-	9.6	-	100	100

[a]**General reaction conditions**: V = 150 mL, $N_{stirrer}$ = 1000 rpm, $c_{Glycerol}$ = 15 wt %, $m_{catalyst}$ = 1.00 g, solvent: H_2O. **Reaction conditions** for the first step: T = 230 °C, $p(N_2)$ = 30 bar, t = 7 h. **Reaction conditions** for the second step: T = 140 °C, $p(H_2)$ = 25 bar, $p(H_2)$ = 5 bar, t = 1 h.

estimates are in very good agreement, while the confidence intervals in Table 2 and the confidence ellipsoids shown in the ESI (Figures S14 and S16) illustrate the correlation of the parameters in the nonlinear kinetic models.

As highlighted by the simulated concentration profiles for the dehydration step (cf. Figure 11) as well as for the hydrogenation step (cf. Figure 12), the kinetic model does yield a good agreement with the experimental data.

Two-Step Separated Approach

To show that the reaction can indeed be separated, a proof-of-concept experiment was conducted. For each step, the previously determined optimal reaction conditions were used. The first step (glycerol dehydration) was conducted using a 15 wt % glycerol-in-water solution at 230 °C under 30 bar nitrogen to prevent the formation of ethylene glycol through C−C cleavage. Subsequently, the reaction solution was cooled to 140 °C, the gas phase was exchanged to hydrogen, and the second acetol hydrogenation step was conducted at 140 °C under 25 bar partial hydrogen pressure (30 bar total pressure) to prevent subsequent hydrogenolysis of 1,2-PDO. The results of this experiment are shown in Table 3.

During the first step of the reaction, a 13.4% conversion of glycerol reaching 9.0% acetol and 0.6% 1,2-PDO, with selectivities of 67.0% and 4.4%, respectively, was achieved. Afterward, all the acetol formed during the first step was hydrogenated to 1,2-PDO during the second step of the reaction. As expected, glycerol was only consumed during the dehydration step of the reaction, while some 1,2-PDO was also formed. These results demonstrate that the two reaction steps can be effectively combined in a single unit operation. C−C cleavage products, such as ethylene glycol and methane, and decomposition products, such as *n*-propanol and ethanol, observed in the conventional one-step approach in previous studies[12−18] were not detected here. This highlights that the separated approach effectively suppresses the undesired side product formation.

However, only 71.4% of the consumed reactant could be identified. To answer the question, if this loss results from glycerol undergoing a side reaction or acetol decomposing, a stability experiment using a glycerol (14 wt %) and acetol (1 wt %) mixture in water was conducted using the same reaction conditions as the first step of the two-step experiment. The concentrations were chosen to yield a mixture similar to that

https://doi.org/10.1021/acs.iecr.6c00905
Ind. Eng. Chem. Res. XXXX, XXX, XXX−XXX

obtained after the first reaction step. The resulting temporal conversion and yield graph is shown in Figure 13.

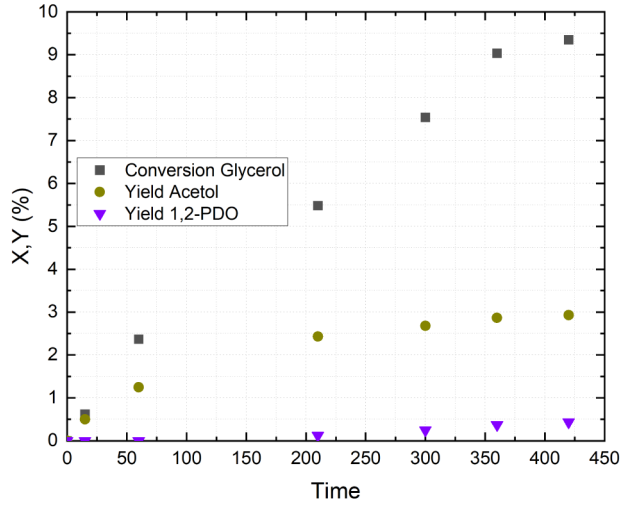

Figure 13. Conversion (X), yield (Y), and carbon balance for the stability experiment using a glycerol (14 wt %) acetol (1 wt %) mixture in water. Reaction conditions: V = 150 mL, T = 230 °C, $p_0(N_2)$ = 30 bar, t = 7 h, c_{gly} = 14 wt %, c_{acetol} = 1 wt %, $N_{stirrer}$ = 1000 rpm, $m_{catalyst}$ = 1.00 g, solvent: H_2O.

While glycerol conversion increases almost linearly throughout the reaction up to 9.3%, the product yields do not. The acetol yield increases first quickly to 1.2% after 60 min, before flattening out over the course of the experiment, ending in 2.9% after 420 min. 1,2-PDO is only found from 210 min onward during the experiment, and only in small amounts up to 0.4% after 420 min. That glycerol consumption remains linear, while acetol yield flattens, suggests that acetol decomposes under the applied reaction conditions, asking for immediate hydrogenation of the intermediate acetol once it is formed. This will be one of the major tasks for the future SMART reactor, ensuring high adaptivity and resilience. As the stability experiments (Figure S8) show, acetol undergoes thermal decomposition under the applied reaction conditions, primarily forming a second oil phase. However, since the acetol concentration in the catalytic experiments is significantly lower than that in the stability experiment, only water-soluble oligomers, rather than a water-insoluble oil, are formed. Because of their low concentration and broad molecular weight distribution, the oligomers could not be identified.

One way to limit acetol decomposition is to monitor the reaction in real time. This enables automated switching from the dehydration step to the hydrogenation step before acetol decomposition outpaces acetol formation. While the HPLC used in this study is too slow to achieve real-time resolution, other analytical methods such as *operando* IR spectroscopy can fulfill this role. However, these require significant monetary investment. pH measurements, however, are significantly cheaper to implement and can monitor the dehydration to acetol as shown in Figure S19. Herein, the pH drops throughout the reaction, as acetol is formed. This is because acetol is significantly more acidic than glycerol and 1,2-PDO. The pH drop can then be used to determine the reaction progress, enabling switching at an optimal moment.

CONCLUSION

This work demonstrates a strategy for making the glycerol hydrogenolysis SMART by separating both reaction steps demanding for very different conditions with respect to gas atmosphere and temperature range as a key for tailoring selectivity and reaction control. Both external and internal mass and heat transfer limitations could be excluded for the first endothermic glycerol dehydration step under the applied reaction conditions, allowing for deducing the kinetic parameters in the reaction-controlled regime. Consequently, the kinetics for the glycerol hydrogenolysis step have been determined by varying the initial glycerol concentration revealing a reaction order of 0.27 for glycerol and an optimized initial glycerol concentration of 15 wt %, whereby varying the reaction temperature shows a sweet spot at 230 °C giving an effective activation energy of about 43 kJ mol^{-1}. With respect to the second acetol hydrogenation step, COSMO-RS predictions estimated the Henry's law volatility constant of hydrogen both in acetol/water and in glycerol/water mixtures excluding mass transfer limitations and giving a reaction order of 2.15 for hydrogen and around zero with respect to acetol. Moreover, an acetol concentration of 7.5 wt % using 25 bar hydrogen at 140 °C was determined as the optimum reaction parameters. Again, external heat transfer limitation could be excluded showing an activation energy of about 57 kJ mol^{-1}. Based on the analysis of the confidence ellipsoids it should however be borne in mind that the pre-exponential factor and the activation energy are strongly correlated. While the OFAT approach yields slightly higher reaction orders compared to the NLR-based parametrization, both parameter sets provide a good approximation of the experimental data based on the kinetic models for both the dehydration and the hydrogenation step confirming that the models reliably reproduce the observed reaction behavior.

ASSOCIATED CONTENT

Data Availability Statement

Research data is available after the official publication (10.15480/882.16747).

Supporting Information

The Supporting Information is available free of charge at https://pubs.acs.org/doi/10.1021/acs.iecr.6c00905.

PID of experimental setup, HPLC calibration curves, determination of standard deviation, temporal concentration profiles for both reaction steps, conversion, yield, and selectivity profiles over time for both reaction steps, methodology for kinetic modeling, methodology for estimation of hydrogen solubility (PDF)

AUTHOR INFORMATION

Corresponding Author

Jakob Albert − *Institute of Technical and Macromolecular Chemistry, University of Hamburg, Hamburg 20146, Germany*; orcid.org/0000-0002-3923-2269; Email: jakob.albert@uni-hamburg.de

Authors

Piet Hassenstein − *Institute of Technical and Macromolecular Chemistry, University of Hamburg, Hamburg 20146, Germany*

https://doi.org/10.1021/acs.iecr.6c00905
Ind. Eng. Chem. Res. XXXX, XXX, XXX−XXX

Jan-Dominik H. Krueger − *Institute of Technical and Macromolecular Chemistry, University of Hamburg, Hamburg 20146, Germany*
Leandros Paschalidis − *Institute of Process Systems Engineering, Hamburg University of Technology, Hamburg 21073, Germany*
Dorothea Voß − *Institute of Technical and Macromolecular Chemistry, University of Hamburg, Hamburg 20146, Germany;* orcid.org/0000-0003-1693-8012
Mirko Skiborowski − *Institute of Process Systems Engineering, Hamburg University of Technology, Hamburg 21073, Germany;* orcid.org/0000-0001-9694-963X

Complete contact information is available at: https://pubs.acs.org/10.1021/acs.iecr.6c00905

Notes

The authors declare no competing financial interest.

■ ACKNOWLEDGMENTS

This project was funded by the Deutsche Forschungsgemeinschaft (DFG, German Research Foundation)—SFB 1615—503850735. We thank KremsChem Austria GmbH for providing high-purity acetol free of charge for this work. We also thank Nanning Jaeschke, Simon Müller, and Irina Smirnova for the estimation of hydrogen solubility in water-acetol and water-glycerol mixtures using COSMO-RS.

■ REFERENCES

(1) Behr, A.; Seidensticker, T. Das Koppelprodukt Der Oleochemie. In *Einführung in die Chemie nachwachsender Rohstoffe: vorkommen, Konversion, Verwendung*; Springer: Berlin, Heidelberg, 2018, pp. 85−105.DOI: .
(2) Wirth, I. C.; Niehaus, D.; Voß, D.; Schlüter, M.; Albert, J. Advanced Glycerol Oxidation to Formic Acid in a Multiphasic Jet Loop Reactor Using Polyoxometalate Catalysts. *ACS Sustainable Chem. Eng.* **2026**, *14* (1), 551−565.
(3) Oliveira, G. N.; Barbosa, N. C.; Araújo, F. C.; Souza, P. H. G.; Soares, A. V. H.; Peixoto, F. C.; Carneiro, J. W. M.; Passos, F. B. Conversion of Glycerine into 1,2-Propanediol for Industrial Applications. In *Jatropha, Challenges for a New Energy Crop*; Springer: Singapore, 2019, pp. 383−414. DOI: .
(4) Kraleva, E.; Palcheva, R.; Dimitrov, L.; Armbruster, U.; Brückner, A.; Spojakina, A. Solid Acid Catalysts for Dehydration of Glycerol to Acrolein in Gas Phase. *J. Mater. Sci.* **2011**, *46* (22), 7160−7168.
(5) Dietz, D.; Zeng, A.-P. Efficient Production of 1,3-Propanediol from Fermentation of Crude Glycerol with Mixed Cultures in a Simple Medium. *Bioprocess Biosyst. Eng.* **2014**, *37* (2), 225−233.
(6) Christoph, R.; Schmidt, B.; Steinberner, U.; Dilla, W. Glycerol. In *Ullmann's Encyclopedia of Industrial Chemistry*; Wiley-VCH Verlag GmbH & Co. KGaA: Weinheim, Germany, 2000. DOI: .
(7) Modvig, A.; Kumpidet, C.; Riisager, A.; Albert, J. Ru-Doped Wells−Dawson Polyoxometalate as Efficient Catalyst for Glycerol Hydrogenolysis to Propanediols. *Materials* **2019**, *12* (13), 2175.
(8) Główka, M.; Krawczyk, T. New Trends and Perspectives in Production of 1,2-Propanediol. *ACS Sustainable Chem. Eng.* **2023**, *11* (19), 7274−7287.
(9) Wang, Y.; Zhou, J.; Guo, X. Catalytic hydrogenolysis of glycerol to propanediols: a review. *RSC Adv.* **2015**, *5* (91), 74611−74628.
(10) Gatti, M.; Pompeo, F.; Nichio, N.; Santori, G. Crude Glycerol Hydrogenolysis to Bio-Propylene Glycol: Effect of Its Impurities on Activity, Selectivity and Stability. *Processes* **2023**, *11* (6), 1731.
(11) Dasari, M. A.; Kiatsimkul, P.-P.; Sutterlin, W. R.; Suppes, G. J. Low-Pressure Hydrogenolysis of Glycerol to Propylene Glycol. *Appl. Catal., A* **2005**, *281* (1−2), 225−231.
(12) Hassenstein, P.; Niehaus, D.; Taherkhani, N.; Krueger, J.-D. H.; Voß, D.; Lumpp, D.; Schroeter, B.; Paschalidis, L.; Smirnova, S.; Skiborowski, M.; Albert, J. Boosting the Chemical Hydrogenolysis of Glycerol to 1,2 Propanediol to Almost Perfect Selectivity Using a Multifunctional Ru-Cu Carbon-Nanotube Supported Catalyst. *ACS Sustainable Chem. Eng.* **2026**, *14* (15), 7559−7574.
(13) Zhang, D.; Cao, Y.; Zhang, P.; Liang, J.; Xue, K.; Xia, Y.; Qi, Z. Investigation of the thermal decomposition mechanism of glycerol: the combination of a theoretical study based on the Minnesota functional and experimental support. *Phys. Chem. Chem. Phys.* **2021**, *23* (36), 20466−20477.
(14) Gatti, M. N.; Perez, F. M.; Santori, G. F.; Pompeo, F. Mechanism Analysis and Chemical Equilibrium Modelling for Liquid Phase Glycerol Hydrogenolysis. *Chem. Thermodyn. Therm. Anal.* **2025**, *18*, 100186.
(15) Miyazawa, T.; Kusunoki, Y.; Kunimori, K.; Tomishige, K. Glycerol Conversion in the Aqueous Solution under Hydrogen over Ru/C + an Ion-Exchange Resin and Its Reaction Mechanism. *J. Catal.* **2006**, *240* (2), 213−221.
(16) Wang, J.; Shen, S.; Li, B.; Lin, H.; Yuan, Y. Ruthenium Nanoparticles Supported on Carbon Nanotubes for Selective Hydrogenolysis of Glycerol to Glycols. *Chem. Lett.* **2009**, *38* (6), 572−573.
(17) Feng, J.; Fu, H.; Wang, J.; Li, R.; Chen, H.; Li, X. Hydrogenolysis of Glycerol to Glycols over Ruthenium Catalysts: Effect of Support and Catalyst Reduction Temperature. *Catal. Commun.* **2008**, *9* (6), 1458−1464.
(18) Zhao, H.; Zheng, L.; Li, X.; Chen, P.; Hou, Z. Hydrogenolysis of Glycerol to 1,2-Propanediol over Cu-Based Catalysts: A Short Review. *Catal. Today* **2020**, *355*, 84−95.
(19) Guo, L.; Zhou, J.; Mao, J.; Guo, X.; Zhang, S. Supported Cu Catalysts for the Selective Hydrogenolysis of Glycerol to Propanediols. *Appl. Catal., A* **2009**, *367* (1−2), 93−98.
(20) Gallegos-Suarez, E.; Guerrero-Ruiz, A.; Rodriguez-Ramos, I.; Arcoya, A. Comparative Study of the Hydrogenolysis of Glycerol over Ru-Based Catalysts Supported on Activated Carbon, Graphite, Carbon Nanotubes and KL-Zeolite. *Chem. Eng. J.* **2015**, *262*, 326−333.
(21) Sherbi, M.; Wesner, A.; Wisniewski, V. K.; Bukowski, A.; Velichkova, H.; Fiedler, B.; Albert, J. Superior CNT-Supported Bimetallic RuCu Catalyst for the Highly Selective Hydrogenolysis of Glycerol to 1,2-Propanediol. *Catal. Sci. Technol.* **2021**, *11* (20), 6649−6653.
(22) Lumpp, D.; Shaikh, S.; Riebesehl, F.; Ruhmlieb, C.; Kruber, K.; Schroeter, B.; Smirnova, S.; Skiborowski, M.; Fiedler, B.; Albert, J. Multifunctional Carbon-Nanotube Supported Catalysts for Efficient Glycerol Hydrogenolysis to 1,2-Propanediol. *ChemCatChem* **2026**, *18* (5), No. e01748.
(23) Gabrysch, T.; Muhler, M.; Peng, B. The Kinetics of Glycerol Hydrodeoxygenation to 1,2-Propanediol over Cu/ZrO2 in the Aqueous Phase. *Appl. Catal., A* **2019**, *576*, 47−53.
(24) Torres, A.; Roy, D.; Subramaniam, B.; Chaudhari, R. V. Kinetic Modeling of Aqueous-Phase Glycerol Hydrogenolysis in a Batch Slurry Reactor. *Ind. Eng. Chem. Res.* **2010**, *49* (21), 10826−10835.
(25) Vasiliadou, E. S.; Lemonidou, A. A. Kinetic Study of Liquid-Phase Glycerol Hydrogenolysis over Cu/SiO2 Catalyst. *Chem. Eng. J.* **2013**, *231*, 103−112.
(26) Pandhare, N. N.; Pudi, S. M.; Mondal, S.; Pareta, K.; Kumar, M.; Biswas, P. Development of Kinetic Model for Hydrogenolysis of Glycerol over Cu/MgO Catalyst in a Slurry Reactor. *Ind. Eng. Chem. Res.* **2018**, *57* (1), 101−110.
(27) Sharma, R. V.; Kumar, P.; Dalai, A. K. Selective Hydrogenolysis of Glycerol to Propylene Glycol by Using Cu: Zn: Cr: Zr Mixed Metal Oxides Catalyst. *Appl. Catal., A* **2014**, *477*, 147−156.
(28) Chiu, C.; Dasari, M. A.; Suppes, G. J.; Sutterlin, W. R. Dehydration of Glycerol to Acetol via Catalytic Reactive Distillation. *AIChE J.* **2006**, *52* (10), 3543−3548.

(29) Turbomole. *"A Development of University of Karlsruhe and Forschungszentrum Karlsruhe GmbH, 1989−2007*; TURBOMOLE GmbH, 2007.
(30) Dassault Systémes Company *COSMOconf, Version 3.0, COSMOlogic GmbH & Co. KGa*; Dassault Systémes Company.
(31) Mears, D. E. Diagnostic criteria for heat transport limitations in fixed bed reactors. *J. Catal.* **1971**, *20* (2), 127−131.
(32) Ardila, A. A. N.; Arriola-Villaseñor, E.; Barrera-Zapata, R.; Hernández, J.; Fuentes, G. A. Kinetic Study of Liquid-Phase Glycerol Hydrodeoxygenation into 1,2-Propanediol over CuPd/TiO_2 -Na. *ACS Omega* **2023**, *8* (17), 14907−14914.
(33) Han, Z.; Fina, A. Thermal conductivity of carbon nanotubes and their polymer nanocomposites: A review. *Prog. Polym. Sci.* **2011**, *36* (7), 914−944.
(34) Vikla, A. K. K.; Koichumanova, K.; He, S.; Seshan, K. Aqueous-Phase Reforming of Hydroxyacetone Solution to Bio-Based H2 over Supported Pt Catalysts. *Green Energy Environ.* **2024**, *9* (4), 777−788.
(35) Sander, R. Compilation of Henry's Law Constants (Version 5.0.0) for Water as Solvent. *Atmos. Chem. Phys.* **2023**, *23* (19), 10901−12440.
(36) Eckert, F.; Klamt, A. Fast Solvent Screening via Quantum Chemistry: COSMO-RS Approach. *AIChE J.* **2002**, *48* (2), 369−385.
(37) Klamt, A.; Jonas, V.; Bürger, T.; Lohrenz, J. C. W. Refinement and Parametrization of COSMO-RS. *J. Phys. Chem. A* **1998**, *102* (26), 5074−5085.
(38) Klamt, A. Conductor-like Screening Model for Real Solvents: A New Approach to the Quantitative Calculation of Solvation Phenomena. *J. Phys. Chem.* **1995**, *99* (7), 2224−2235.
(39) Hernández-Bravo, R.; Oviedo-Roa, R.; Martínez-Magadán, J.-M.; Aguilar-Cisneros, H.; Domínguez-Esquivel, J. M. H_2 Solubility in Hydrocarbons Calculated by the COSMO-RS Method. *Ind. Eng. Chem. Res.* **2019**, *58* (27), 12361−12368.

https://doi.org/10.1021/acs.iecr.6c00905
Ind. Eng. Chem. Res. XXXX, XXX, XXX−XXX